Influence of QD photosensitizers in the photocatalytic production of hydrogen with biomimetic [FeFe]-hydrogenase. Comparative performance of CdSe and CdTe

Juan Corredor, Dulanjan Harankahage, Frédéric Gloaguen, Maria Rivero, Mikhail Zamkov, Inmaculada Ortiz

Influence of QD photosensitizers in the photocatalytic production of hydrogen with biomimetic [FeFe]-hydrogenase. Comparative performance of CdSe and CdTe

Juan Corredor [a], Dulanjan Harankahage [b], Frederic Gloaguen [c], Maria J. Rivero [a], Mikhail Zamkov [b], Inmaculada Ortiz [a*]

[a] Department of Chemical and Biomolecular Engineering, ETSIIT, University of Cantabria, Avda. de los Castros s/n, 39005, Santander, Spain

[b] Department of Physics and Center for Photochemical Sciences, Bowling Green State University, Bowling Green, Ohio 43043, USA

[c] UMR 6521, CNRS, Université de Bretagne Occidentale, CS 93837, 29238 Brest, France

* Corresponding author. E-mail address: inmaculada.ortiz@unican.es (I. Ortiz)

Highlights:

- Photocatalytic hydrogen production system with [Fe-Fe]H_2-ase mimic, and CdSe or CdTe QDs as photosensitizers.
- Comparison of CdSe and CdTe QDs performance as photosensitizers
- CdSe showed the best performance for hydrogen production.
- Electron transfer rate from ascorbic acid to QDs and from QDs to catalysts has been investigated.
- Electron transfer rate from ascorbic acid to QDs was found as rate limiting step.

Abstract

Photocatalytic systems comprising a hydrogenase-type catalyst and CdX (X = S, Se, Te) chalcogenide quantum dot (QD) photosensitizers show extraordinary hydrogen production rates under visible light excitation. What remains unknown is the mechanism of energy conversion in these systems. Here, we have explored this question by comparing the performance of two QD sensitizers, CdSe and CdTe, in photocatalytic systems featuring aqueous solutions of a [Fe_2 (μ-1,2-benzenedithiolate) CO_6] catalyst

and an ascorbic acid sacrificial agent. Overall, the hydrogen production yield for CdSe-sensitized reactions QDs was found to be 13 times greater than that of CdTe counterparts. According to emission quenching experiments, an enhanced performance of CdSe sensitizers reflected a greater rate of electron transfer from the ascorbic acid (k_{Asc}). The observed difference in the QD-ascorbic acid charge transfer rates between the two QD materials was consistent with respective driving forces for these systems, determined from cyclic voltammetry measurements.

Keywords: Photocatalytic hydrogen production, hydrogenase mimic, quantum dot, CdSe, CdTe, electron transfer, hybrid systems.

1. Introduction

In the current global context, greenhouse gas emissions due to the combustion of fossil fuels pose a threat to the global climate change (Fang et al., 2018; Hinojosa-Reyes et al., 2017; Seadira et al., 2018). Therefore, research efforts have been directed towards finding alternative and environmentally-friendly energy sources. In this context, hydrogen appears as a clean energy vector whose combustion only produces water (Chen et al., 2018; Munfarida et al., 2020; Oh et al., 2020). Nowadays, it is mainly produced by steam reforming from fossil fuels (Chu et al., 2017; Corredor et al., 2020a; Nikolaidis and Poullikkas, 2017). This process is energy intensive and plagued by the emission of greenhouse gases (Holladay et al., 2009; Ribao et al., 2019). As a result, the potential to produce hydrogen from alternative and greener technologies, where electrolysis takes the leading role, is becoming increasingly important. Complementarily, hydrogen can be released from residual gas or liquid effluents through the use of cost-effective technologies, such as photocatalysis (Nasir et al., 2019;

Rivero et al., 2019; Yue et al., 2017). Photocatalysis is a way to harvest sunlight energy and store it in the form of solar fuels, just as nature has done through natural photosynthesis (Christoforidis and Fornasiero, 2017; El-Khouly et al., 2017; Lewis S. Nathan, 2016; Zamkov, 2017).

As an alternative to noble metal catalysts, (Cho et al., 2021; Lai et al., 2021; Y. Yang et al., 2021), recent studies have explored heterogeneous photocatalytic systems comprising hydrogenases catalysts and semiconductor quantum dot (QD) photosensitizers. The hydrogen production rates for these materials approaching 2 mmol $H_2 \cdot g_{cat}^{-1} \cdot h^{-1}$ were below those of homogeneous catalysts but showed an impressive long-term stability (Elsayed et al., 2021; Putri et al., 2020; J. Yang et al., 2021).

Hydrogenase mimics is another promising noble metal-free catalyst that shows compelling hydrogen production performance (Fukuzumi et al., 2018; Trincado et al., 2014). Hydrogenases in nature are enzymes, which active sites are composed of Fe and/or Ni, synthesized by certain bacteria and algae; these enzymes catalyze the reversible redox reaction of H^+ to H_2 (Hemming et al., 2018; Li et al., 2018; Wang et al., 2012). Among hydrogenases, [Fe-Fe]H_2-ases have shown a very high production activity of hydrogen, about 6000-9000 H_2 molecules per second per active site (Li et al., 2018; Stripp and Happe, 2009; Wang et al., 2019; Wittkamp et al., 2018). Therefore, they have been studied in the last decades and have awakened interest in the synthesis of biomimetic molecules (Ahmed et al., 2018; Capon et al., 2004; Liu and Darensbourg, 2007; Orain et al., 2014; Quentel et al., 2012; Roy et al., 2013).

[Fe-Fe]H_2-ases photocatalytic hydrogen production systems containing metal complexes, such as $[Ru(bpy)_3]^{2+}$ (bpy = 2,2'-bipyridine) or $[Re(4,4'\text{-dimethylbpy})(CO)_3]^+$ (Na et al., 2008; Pullen et al., 2013; Streich et al., 2010; Wang et al., 2010; Yu et al., 2013) or organic dyes such as Eosin Y or Rose Bengal as

photosensitizers have been extensively studied (Li et al., 2012; Orain et al., 2014; Supplis et al., 2018). Orain et al studied the photocatalytic hydrogen production in aqueous solutions with [Fe-Fe]H_2-ase mimics, and organic dyes as photosensitizers (Orain et al., 2014). Despite promising performance, their main drawback was the fast excitation decay and the spectrally-narrow absorption band of dye sensitizers. In order to overcome these issues, semiconductor QDs have been employed as photosensitizers (Jian et al., 2016; Liang et al., 2015; Song et al., 2014; Troppmann and König, 2016; Wang et al., 2013, 2011; M. Wang et al., 2015; Wen et al., 2017, 2016). Jian et al. compared the performance of $[Ru(bpy)_3]^{2+}$ and CdSe QDs as a photosensitizer for the same aqueous system achieving a hydrogen production rate of 301 and 20840 mmol $H_2 \cdot g_{cat}^{-1} \cdot h^{-1}$, respectively, duplicating the stability of the system. Hydrogen production was further enhanced by using a sacrificial agent that acted as an electron donor, such as ascorbic acid (Figure 1) (Goy et al., 2017).

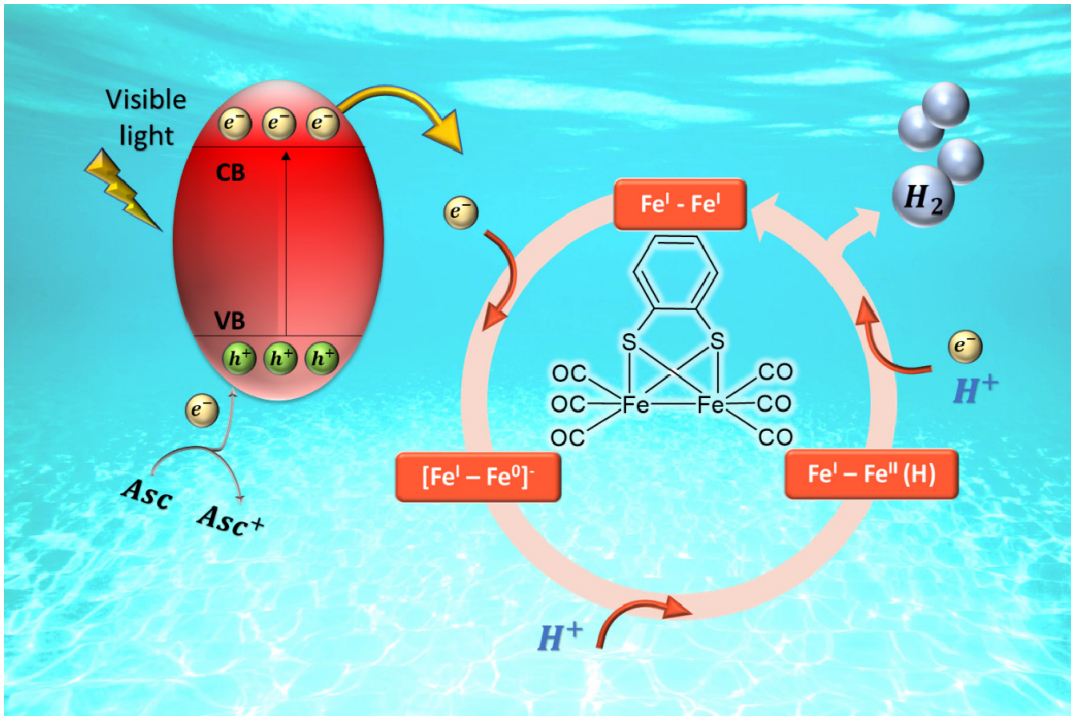

Figure 1. Hydrogen production by a [FeFe]H_2-ase mimic from ascorbic acid aqueous solution with QDs as photosensitizer.

The selection of the QD material for sensitizing hydrogen production is still a challenge. Cadmium chalcogenides, CdS, CdSe and CdTe, are good candidates due to their visible-range absorbance and energetically favorable positions of band edges for driving the hydrogen production processes. Since CdS absorbs the smallest fraction of the solar energy, CdSe and CdTe QDs, exhibiting absorption in the visible and near-IR, are usually preferred. For instance, CdSe has been used as photosensitizer for hydrogen generation in combination with hydrogenases, hydrogenase mimics, and even with bacteria that produce hydrogenases (Chica et al., 2017; Ding et al., 2019; Hamon et al., 2014; Jian et al., 2016; Li et al., 2013, 2020; Liang et al., 2015; Sanchez et al., 2019a, 2019b; Shen et al., 2013; Troppmann and König, 2016; Wang et al., 2013; Wen et al., 2016). CdTe has been also used for this purpose (Brown et al., 2014, 2010; Greene et al., 2012; Jian et al., 2013; Wang et al., 2011; Wroblewska-Wolna et al., 2020). Overall, the two QD sensitizers appeared to perform differently in the presence of the same scavenger and catalyst components (Acharya et al., 2011; JACS 2012, 134 (12) , 5627-5636.), which makes this pair of QDs a promising model system for interrogating energy conversion processes in sacrificial hydrogen production reactions.

The present study offers a comprehensive analysis of the hydrogen production performance for CdSe and CdTe QD photosensitizers under visible light irradiation. The photocatalytic systems in present experiments featured a bio-mimetic hydrogenase catalyst and ascorbic acid as a sacrificial agent. By drawing a comparison between the two sensitizer QDs, we were able to infer that the primary rate-limiting step in these systems is an electron transfer between the sacrificial agent and semiconductor QDs. This conclusion was supported by cyclic voltammetry measurements showing a larger

118 difference between the oxidation potential of ascorbic acid and the valence band of
119 CdSe, as compared to CdTe.

120

121 ## 2. Materials and methods

122 ### 2.1. Materials

123 Oleic acid (OA) 90%, 1-octadene (ODE) 90%, trioctylphosphine oxide (TOPO),
124 cadmium oxide (CdO) 99.5%, tellurium powder 99.8% and tributylphosphine 97%
125 (TBP) were purchased from Sigma Aldrich. Chloroform and acetone were purchased
126 from ChemPure Chemicals. L-Ascorbic acid 98+% and methanol were provided by
127 Alfa Aesar. N-octadecylphosphonic acid (ODPA) was supplied by PCI.
128 Trioctylphosphine (TOP) was purchased from Strem Chemicals Inc. Selenium powder
129 99.99% was supplied by Beantown Chemicals. 3-mercaptopropionic acid (MPA) was
130 acquired from Acros Organics. Sodium dodecyl sulfate (SDS) 10% was provided by
131 LifeTechnologies.

132 ### 2.2. Hydrogenase synthesis

133 [Fe_2(μ-1,2-benzenedithiolate)$(CO)_6$], the [Fe-Fe]H_2-ase mimic, was synthesized as
134 previously described in the literature (Cabeza et al., 1998).

135 ### 2.3. Synthesis of CdSe and CdTe quantum dots

136 OA-capped CdSe QDs were synthesized according to a procedure adapted from the
137 literature (Mongin et al., 2018). Briefly, OA-capped CdSe QDs were synthesized from
138 cadmium and selenium solutions. To prepare cadmium solution, 180 mg of CdO were
139 dissolved with 75 mg of ODPA, 9 g of TOPO and 6 mL of OA in a flask at 300 ºC
140 under Ar atmosphere. When the solution turned clear, 5.4 mL of TOP were added.
141 Selenium solutions were prepared with 180 mg of Se powder and 3 mL of TOP at 140

ºC under Ar atmosphere. When selenium was dissolved, the solution was cooled down to 80ºC and it was injected into the cadmium solution. The reaction time was 2 min. Every step was performed under magnetic stirring.

To synthetize ODPA-capped CdTe QDs, the cadmium solution was prepared with 25.6 mg of CdO, 147.2 mg of ODPA and 8 mL of ODE at 300 ºC under Ar atmosphere. Tellurium solution was prepared from 51 mg of tellurium powder, 4 mL of ODE, and 0.46 mL of TBP at 80 ºC under Ar atmosphere. Tellurium solution was injected into the cadmium solution and the reaction was carried out for 4.75 min.

Both CdTe and CdSe solutions were centrifuged for 4.5 min at 6500 rpm after adding ethanol:acetone solution, with a volume ratio 2:1, to cause precipitation of the crystals. The ratio between the crystals solution and the ethanol-acetone mixture was 1:3 in volume. The precipitated crystals were re-dissolved in chloroform.

The ligand exchange process was carried out according to a procedure adapted from the literature (Chang et al., 2016). Briefly, 0.5 mL of MPA were dissolved in 10 mL of a 1:1 methanol:chloroform solution at basic pH. 1.5 mL of crystals solution were added under constant stirring. QDs precipitated after centrifugation in acetone. They were dissolved in water and re-precipitated in acetone. Finally, the QDs were dissolved and stored in water.

2.4. Materials characterization

^{1}H NMR spectra of [Fe_2(μ-1,2-benzenedithiolate)$(CO)_6$] in deuterated acetone were recorded on a Bruker AC-300 FT-NMR spectrometer and were referenced against $SiMe_4$. The infrared spectra of [Fe_2(μ-1,2-benzenedithiolate)$(CO)_6$] in hexane were recorded on a Nicolet Nexus FT-IR spectrometer.

The materials absorbance spectra were recorded in a UV-Vis spectrophotometer Cary 60 (Agilent). Photoluminescence spectra and excitation decay lifetime (τ_0) of CdSe and CdTe QDs were obtained, exciting them with 405 nm PicoQuant PDL 800-D pulsed laser and measuring their emission with an AndornewtonEM SR-303i-A spectrograph.

2.5. Hydrogen production

Hydrogen production experiments were carried out in an 8 mL reactor under magnetic stirring. The reaction medium consisted of 4 mL of aqueous solution with ascorbic acid 200 mM (excess of the sacrificial agent was used to avoid its influence on the kinetics of hydrogen production), 0.1 mM of [Fe-Fe]H_2-ase mimic, QDs in a concentration between 0.001 mM and 0.1 mM, and 10 mM SDS sodium dodecyl sulfate (SDS) to solubilize the [Fe-Fe]H_2-ase mimic (Orain et al., 2014; Supplis et al., 2018). The light source consisted of a 150 W halogen lamp, provided with a filter which allowed only visible light to pass (400 nm < λ < 800 nm). The irradiance on the reactor wall was 31 $mW \cdot cm^{-2}$. It was measured with a Compact Power and Energy Meter Console PM100D from Thorlabs. The concentration of hydrogen was measured with a Shimadzu 8A gas chromatograph, equipped with a thermal conductivity detector and a molecular sieve column 80/100 using argon as a carrier gas. Hydrogen production experiments were performed at pH 4.5, which is close to the ascorbic acid pK_a (4.2) (Tu et al., 2017); it has been reported that working close to the sacrificial agent pK_a enhances hydrogen production (Corredor et al., 2019).

3. Results

The [Fe-Fe]H_2-ase mimic [Fe_2(μ-1,2-benzenedithiolate)$(CO)_6$] was characterized by FTIR and ^{1}H-NMR spectroscopy. Three bands were displayed in the infrared spectra in

189 the ν_{CO} region: 2006, 2045 and 2079 cm^{-1}. ^{1}H-NMR (300 MHz, $(CD_3)_2CO$): δ 7.24 (m,
190 2H), 7.46 (m, 2H). These data are in good agreement with those reported by Cabeza et
191 al. (Cabeza et al., 1998). The [Fe-Fe]H_2-ase mimic absorbance spectra (Figure S1)
192 showed an absorption peak at 330 nm and absorption at wavelengths lower than 300
193 nm. Therefore, the catalyst did not absorb radiation during hydrogen production
194 experiments, which were carried out using visible light excitation (400-800 nm).

195 The influence of the QD diameter on the effectiveness of hydrogen production with
196 hydrogenase enzymes has been investigated previously (Brown et al., 2014). In this
197 work, we only focus on single sizes of CdTe and CdSe QDs (2.95 nm and 2.68 nm,
198 respectively, see Figure S2. Yu et al., 2003), which were chosen to enable similar
199 extinction values for the two sensitizers in the visible range. In this size range, the rate
200 of electron transfer to a catalysis was not expected to be influenced by the particle size
201 (Brown et al., 2014).

202 The UV-Vis absorbance and the emission spectra of the synthesized CdSe and CdTe
203 QDs before and after the ligand exchange process are shown in Figure 2. A slight blue-
204 shift was observed in the absorbance peak of both materials when the hydrophobic
205 ligands were exchanged with MPA.

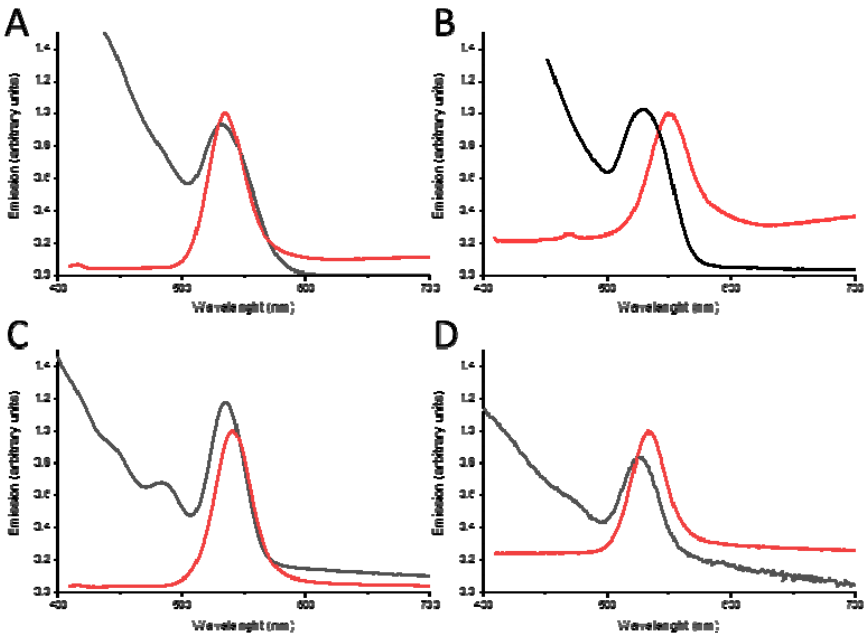

206

207 *Figure 2. CdSe and CdTe absorption (black) and emission (red) spectra of: (A) CdSe-OA; (B)*
208 *CdSe-MPA; (C) CdTe-ODPA; (D) CdTe-MPA.*

209

210 Figure 3 shows the time-resolved luminescence decay curves of excited CdSe-OA,
211 CdSe-MPA, CdTe-ODPA and CdTe-MPA. The fluorescence intensity decay lifetime
212 (τ_0) was calculated by fitting the data to a three-phase exponential decay function (Gong
213 et al., 2013). The τ_0 values for CdSe-OA, CdSe-MPA, CdTe-ODPA and CdTe-MPA
214 were determined to be 38.4, 2.6, 14.7 and 9.6 ns, respectively. The value of τ_0 decreases
215 upon the ligand exchange with MPA for both materials. This decrease was previously
216 explained by the photoinduced hole transfer from a nanocrystal to MPA, which exhibits
217 a more negative energy relative to the semiconductor valence band (Ben-Shahar et al.,
218 2015; P. Wang et al., 2015).

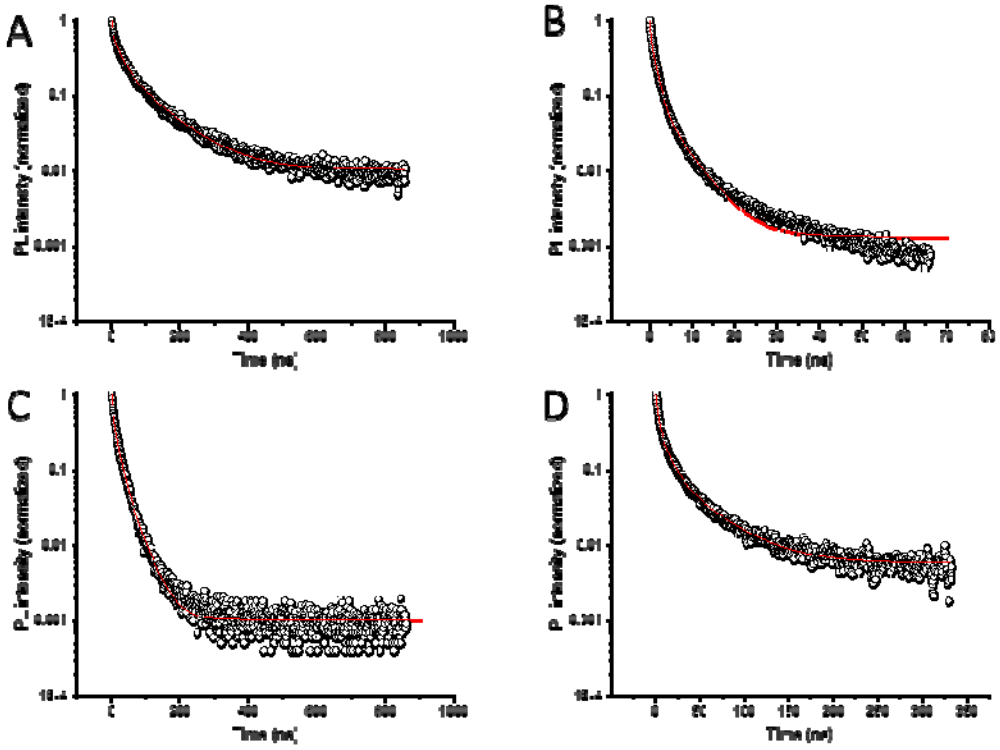

Figure 3. Time-resolved photoluminescence decay spectra for (A) CdSe-OA, (B) CdSe-MPA, (C) CdTe-ODPA and (D) CdTe-MPA.

3.2. Influence of Photosensitizer concentration on hydrogen production

Control tests were carried out in the dark and in the absence of a catalyst and photosensitizers successfully confirming the absence of hydrogen production. In the next step, the influence of the CdSe QD concentration on hydrogen production was investigated in the 0.001 mM to 0.1 mM range. The pH of the solution was the natural pH of the ascorbic acid (pKa 4.2) (Tu et al., 2017), as the optimal pH for these systems has a value close to the pK_a of the sacrificial agent. In addition, Gloaguen and coworkers reported that a pH between 3 and 6 favored the protonation of the electrochemically reduced [Fe-Fe]H_2-ase mimic leading to higher hydrogen production (Quentel et al., 2012). The selected concentration of ascorbic acid was 200 mM

following previous reports (Jian et al., 2016). Figure 4 shows that the highest amount of hydrogen was produced using [CdSe] = 0.01 mM, giving a turnover number (TON) of 18.3 mol of H_2 produced per mol of [Fe_2(μ-1,2-benzenedithiolate)$(CO)_6$] during 3 h. The corresponding turnover number frequency (TOF), measured in mol of produced H_2 per mol of catalyst per unit of time, was 6.5 h^{-1}. Under the conditions of this study, the generated hydrogen increased with the QD concentration up to a maximum value obtained at a concentration of CdSe 0.01M, and after that it decreased as the concentration of the QD increased.

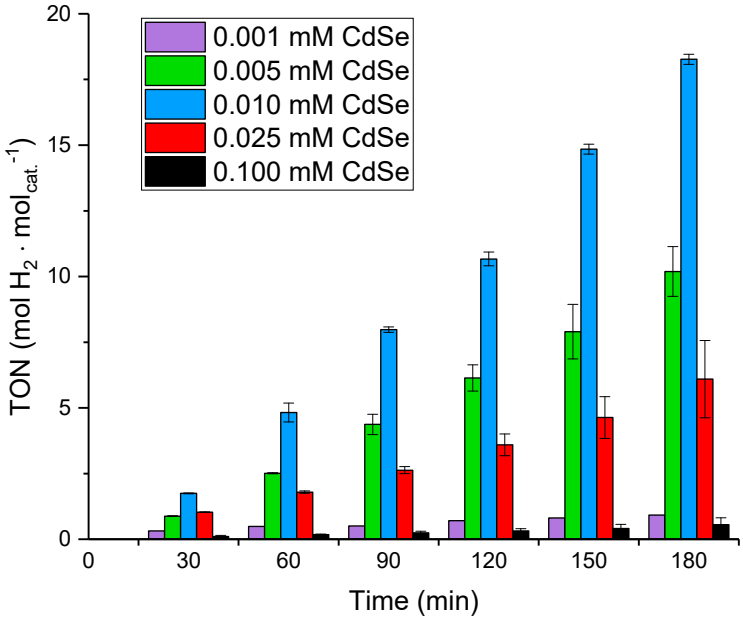

Figure 4. Hydrogen production for different CdSe-MPA concentrations. [Ascorbic acid]: 200 mM, [Fe_2(μ-1,2-benzenedithiolate)$(CO)_6$]: 0.1 mM, pH: 4.5.

Further insights into the influence of the CdSe QD concentration on hydrogen generation are provided in Figure S3, which shows the number of excited CdSe particles per second versus the total number of CdSe nanoparticles in the solution. The procedure for estimating the number of excited QDs is given in SI, together with the

absorption spectra of QD solutions (Figure S4) and the excitation spectrum (Figure S5). The dashed line in Figure S3 shows an ideal case in which the average number of excited nanoparticles approaches that of the nanoparticles in solution. These conditions are observed when the concentration of the photosensitizer is less than 0.01 mM. However, only about 75% and 20% of the total particles were excited for QD concentrations of 0.025 mM and 0.1 mM, respectively. Therefore, the decrease in hydrogen production for concentrations of CdSe greater than 0.01 mM was attributed to the inefficient activation of the photosensitizer particles. This is clarified by equation S6, which shows that the irradiation of the light source strongly influences the optimal concentration of the photosensitizer because the number of excited particles depends on the number of accessible photons.

3.3. Comparative performance of the photosensitizers CdSe and CdTe

In order to compare the performance of photosensitizers MPA-CdSe and MPA-CdTe, experiments were carried out with a concentration 0.01 mM of each photosensitizer. Figure 6 shows the data of hydrogen production expressed as TON with CdSe and CdTe during 3 h. Under similar experimental conditions, a TOF of 6.5 h^{-1} was observed with CdSe, which is 13-fold higher than with CdTe (TOF = 0.5 h^{-1}). Table S1 collects the values of the total hydrogen production and the production rate.

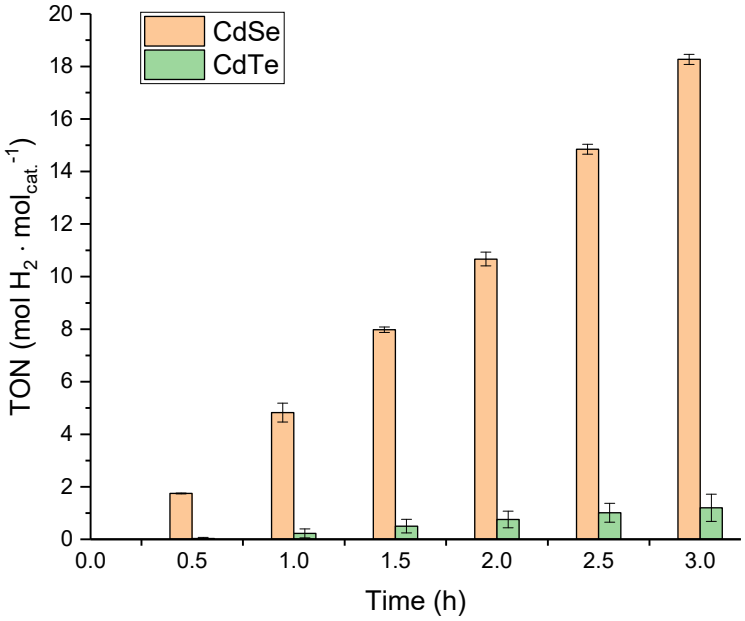

Figure 6. Hydrogen production with CdSe and CdTe as photosensitizers. [Photosensitizer]: 0.01 mM [Ascorbic acid]: 200 mM and [Fe_2(μ-1,2-benzenedithiolate)$(CO)_6$]: 0.1 mM, pH 4.5.

Emission quenching spectra with progressive addition of catalyst and ascorbic acid to CdSe-MPA and CdTe-MPA solutions are shown in Figure 7. According to Figures 7A and 7B, addition of a catalyst causes a decrease in the fluorescence intensity, which is consistent with the transfer of photoexcited electrons from CdSe/CdTe to the catalyst. The comparison of the UV-Vis spectrum of [Fe_2(μ-1,2-benzenedithiolate)$(CO)_6$] (Figure S1), which shows an absorption peak around 340 nm, with the emission spectra of CdSe and CdTe showing maxima around 545 and 540 nm, respectively (Figure 2), leads to the conclusion that the catalyst does not absorb the fluorescence emitted by the photosensitizer. Thus, the loss of fluorescence intensity is due to the transfer of electrons from the conduction band of the photosensitizer to the catalyst. Consequently, the quenching constant (k_q), calculated using the Stern-Volmer equation (Figure S7) (Stern and Volmer, 1919), is equal to the rate constant of electron transfer from the

283 photosensitizer to the catalyst (k_{ET}), k_q=k_{ET}, with values of $1.55 \cdot 10^{12}$ $M^{-1} \cdot s^{-1}$ and
284 $4.02 \cdot 10^{11}$ $M^{-1} \cdot s^{-1}$for CdSe and CdTe, respectively. Similarly, quenching of fluorescence
285 was also observed with increasing concentration of the ascorbic acid (scavenger) in
286 solution (see Figures 7C and 7D). Since there is no overlap between the ascorbic acid
287 absorption (Figure S6) and the photosensitizer emission (Figure 2), it was concluded
288 that the quenching effect is due to the transfer of electrons from ascorbic acid to the
289 photosensitizer valence band. In this case, the rate constant of electron transfer from
290 ascorbic acid to the photosensitizer (k_{asc}), was found to be $5.42 \cdot 10^{9}$ $M^{-1} \cdot s^{-1}$and $4.31 \cdot 10^{8}$
291 $M^{-1} \cdot s^{-1}$ for CdSe and CdTe, respectively.

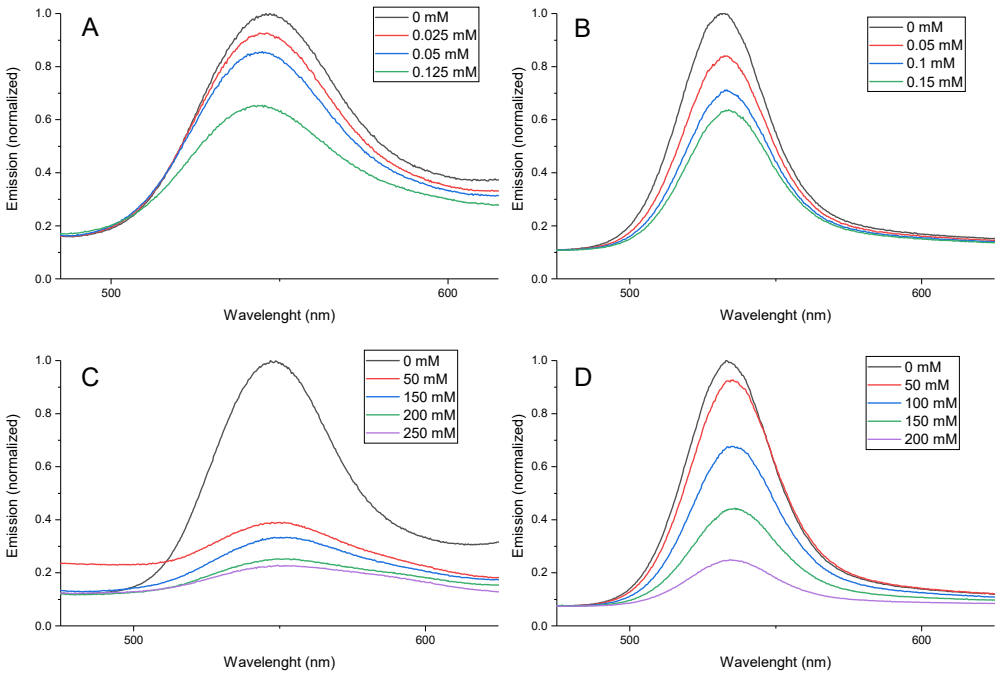

292

293 *Figure 7. Emission spectra at different concentrations of (A) catalyst in CdSe-MPA solution; (B)*
294 *catalyst in CdTe-MPA solution; (C) ascorbic acid in CdSe-MPA solution; (D) ascorbic acid in*
295 *CdTe-MPA solution.*

296

A difference of 2-3 orders of magnitude was observed between k_{ET} and k_{asc} in both materials. This difference agrees with previous reports (Jian et al., 2016; Wen et al., 2016). Figure 8 depicts the proposed mechanism where the electron transfer from ascorbic acid to the valence band of the QDs is the rate-limiting step as k_{asc} is two orders of magnitude smaller than k_{ET}. Furthermore, CdSe sensitizer showed a greater k_{asc} which was nearly 13 times higher than for CdTe. This fact is consistent with the 13 times greater hydrogen production rate obtained with CdSe than with CdTe. Therefore, it was concluded that the electron transfer from the ascorbic acid to the QD was the primary rate-limiting step in hydrogen production reactions.

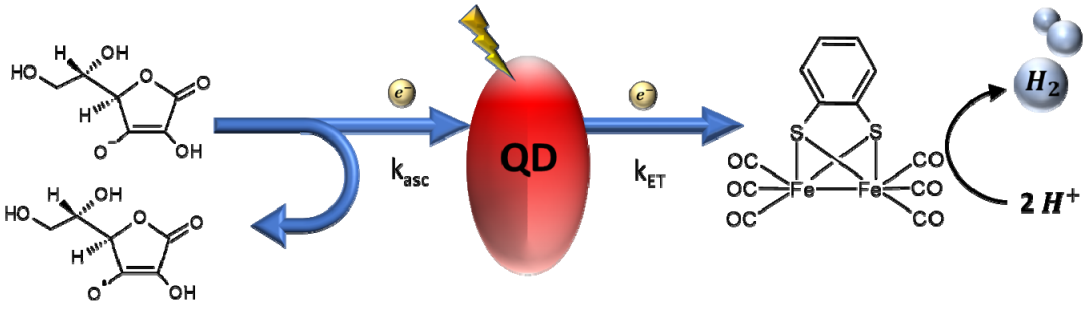

Figure 8. Mechanism of photocatalytic hydrogen production.

Figure 9 represents the energy diagram of both systems at pH 4.5. The reduction potential of the [Fe-Fe]H_2-ase mimic was determined by cyclic voltammetry as $E_{1/2} \sim$ -0.68 V at pH 4.5 (Quentel et al., 2012) and for ascorbic acid the corresponding value was -0.41 V (Tu et al., 2017). Although it is energetically favorable for the ascorbic acid to produce hydrogen directly, it was confirmed experimentally that this redox reaction did not occur. For both semiconductors, Figure 9 illustrates the conduction and valence band edge energies for CdSe and CdTe QDs adjusted for present particle diameters considering the variability range found in literature. (Jasieniak et al., 2011). Notably, the energy difference between the oxidation potential of ascorbic acid and the valence band

of the QD is greater for CdSe than for CdTe, which is consistent with the higher value of k_{Asc} of CdSe with respect to CdTe. This causes a comparatively greater driving force for the photoinduced electron transfer from sacrificial agent to the CdSe.

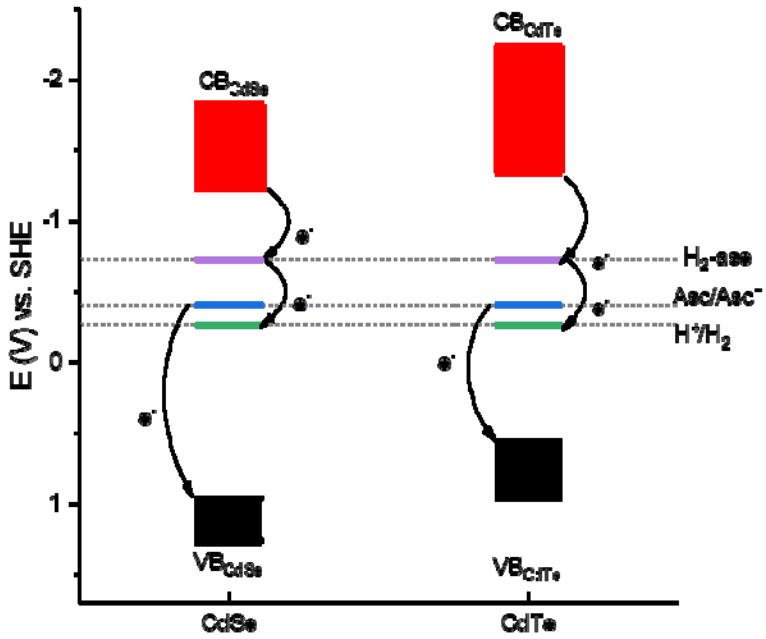

Figure 9. Energy levels at pH 4.5 of CdSe, CdTe, [FeFe]H_2-ase mimic and ascorbic acid.

Overall, the above experiments demonstrate that the rate-limiting step for the hydrogen production in the QD-([FeFe]H_2-ase mimic)-(ascorbic acid) system is the electron transfer from the ascorbic acid (sacrificial agent) to the valence band of the photosensitizer characterized by the kinetic constant k_{Asc}.

In an effort to assess the stability of the investigated catalytic system, several selected experiments were carried out for the duration of 24 h. According to Figure 10A, CdSe reached a TON value of 100 while CdTe achieved a TON value of 3.5 after 24 h. The initial TOF with CdSe was 6.5 h^{-1} decreasing to 1.8 h^{-1} after 18 h while the initial TOF with CdTe was 0.5 h^{-1} decreasing to 0.1 h^{-1} after 18 h. Therefore, hydrogen production

rate decreased about 75% for both materials in this period of time. Figure 10B shows hydrogen production with CdSe operating in different cycles. Cycle 1 shows hydrogen production with a fresh catalyst. Hydrogen production rate decreased to 1.8 h^{-1}after 18 h of reaction. Before starting cycle 2, a purge with argon was carried out in the photoreactor to eliminate any possible inhibitory effect of the product, as has been previously reported (Corredor et al., 2020b). After this purge, the TOF was 1.7 h^{-1}, similar to the value at the end of cycle 1. Therefore, the decrease in hydrogen production was not attributed to the hydrogen inhibitory effect. Next, catalyst deactivation was examined by addition of $7.5 \cdot 10^{-3}$ mM of fresh catalyst at the beginning of cycle 3; hydrogen production recovered similar values to the initial experimental conditions. Therefore, the decline and stop of hydrogen production is attributed to the loss of catalyst activity.

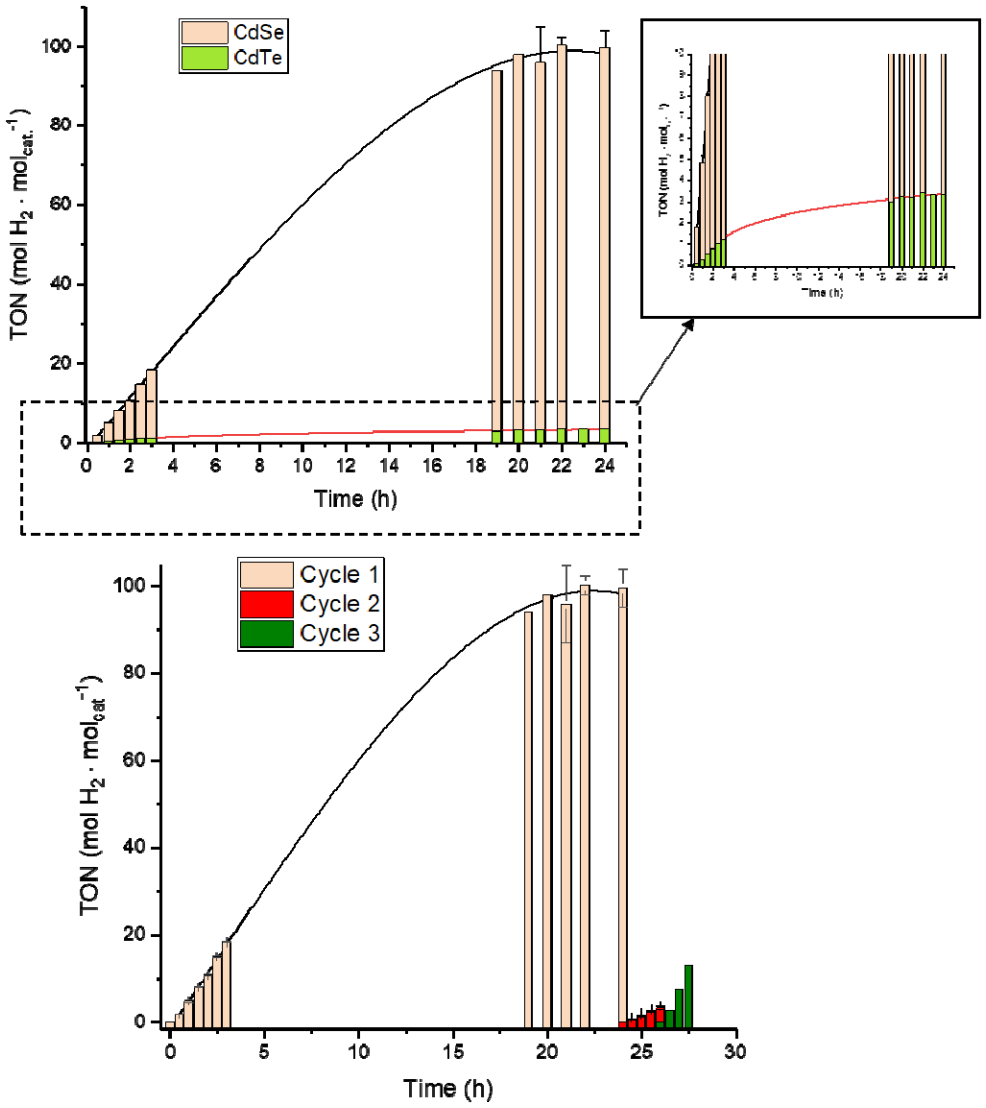

Figure 10. Hydrogen production with (A) CdSe and CdTe for longer operation times, and (B) catalyst reuse with CdSe.

4. Conclusions

In this work, we compare the photocatalytic performance of two QD photosensitizers, CdSe and CdTe, in hydrogen production systems composed of a hydrogenase mimic catalyst and ascorbic acid as sacrificial agent. CdSe QDs showed an overall better performance. For these materials, the highest hydrogen production rate was observed

using 0.01 mM nanoparticle concentration, 200 mM of ascorbic acid, and 0.1 mM of [Fe-Fe]H_2-ase mimic (excitation intensity = 31 $mW \cdot cm^{-2}$ of, 400 nm < λ < 800 nm).

Quenching experiments revealed that the rate of electron transfer from photosensitizer to the catalyst, k_{ET}, is of 2-3 orders of magnitude higher than that of scavenger → photosensitizer transfer process, k_{Asc}. In particular, we found that k_{asc} for CdSe was 13 times greater than that of CdTe. The ratio of hydrogen production rates for the two materials, CdSe and CdTe, exhibited roughly the same ratio (13:1), suggesting that the photoinduced hole transfer from a QD to a scavenger was the rate limiting step. A relatively greater value of k_{asc} for CdSe was attributed to the larger difference between the oxidation potential of ascorbic acid and the valence band energy of CdSe in comparison with CdTe. This conclusion suggests that photosensitizers that enable faster sacrificial regenerations may hold the key to improving the hydrogen production rate. Another important area to be addressed by the future research is the long-term stability of hydrogenase mimic catalysts, which lost 25% of catalytic activity after 18 h in present measurements.

5. Acknowledgements

Financial support from projects RTI2018-099407-B-I00, RTI2018-093310-B-I00, RTC2019-006820-5 (MCIU/AEI/FEDER, UE) and 'HYLANTIC'-EAPA_204/2016 (Interreg Atlantic/FEDER UE) is gratefully acknowledged. Juan Corredor is grateful to FPI contract grant (BES-2016-079201). MZ and DH were supported by the Award DE-SC0016872 (MZ) funded by the U.S. Department of Energy, Office of Science.

6. References

Acharya, K.P., Khnayzer, R.S., O'Connor, T., Diederich, G., Kirsanova, M., Klinkova, A., Roth, D., Kinder, E., Imboden, M., Zamkov, M., 2011. The role of hole localization in sacrificial hydrogen production by semiconductor-metal heterostructured nanocrystals. Nano Lett. 11, 2919–2926. https://doi.org/10.1021/nl201388c

Ahmed, M.E., Dey, S., Darensbourg, M.Y., Dey, A., 2018. Oxygen-Tolerant H_2 Production by [FeFe]-H_2ase Active Site Mimics Aided by Second Sphere Proton Shuttle. J. Am. Chem. Soc. 140, 12457–12468. https://doi.org/10.1021/jacs.8b05983

Baker, D.R., Kamat, P. V., 2010. Tuning the emission of CdSe Quantum Dots by Controlled Deep-Trap Enhancement. Langmuir 26, 11272–11276.

Ben-Shahar, Y., Scotognella, F., Waiskopf, N., Kriegel, I., Dal Conte, S., Cerullo, G., Banin, U., 2015. Effect of surface coating on the photocatalytic function of hybrid CdS-Au nanorods. Small 11, 462–471. https://doi.org/10.1002/smll.201402262

Brown, K.A., Dayal, S., Ai, X., Rumbles, G., King, P.W., 2010. Controlled assembly of hydrogenase-CdTe nanocrystal hybrids for solar hydrogen production. J. Am. Chem. Soc. 132, 9672–9680. https://doi.org/10.1021/ja101031r

Brown, K.A., Song, Q., Mulder, D.W., King, P.W., 2014. Diameter dependent electron transfer kinetics in semiconductor-enzyme complexes. ACS Nano 8, 10790–10798. https://doi.org/10.1021/nn504561v

Cabeza, J.A., Martínez-García, M.A., Riera, V., Ardura, D., García-Granda, S., 1998. Binuclear iron(I), ruthenium(I), and osmium(I) hexacarbonyl complexes containing a bridging benzene-1,2-dithiolate ligand. Synthesis, X-ray structures, protonation reactions, and EHMO calculations. Organometallics 17, 1471–1477.

https://doi.org/10.1021/om970922j

Capon, J.F., Gloaguen, F., Schollhammer, P., Talarmin, J., 2004. Electrochemical proton reduction by thiolate-bridged hexacarbonyldiiron clusters. J. Electroanal. Chem. 566, 241–247. https://doi.org/10.1016/j.jelechem.2003.11.032

Chang, C.M., Orchard, K.L., Martindale, B.C.M., Reisner, E., 2016. Ligand removal from CdS quantum dots for enhanced photocatalytic H_2 generation in pH neutral water. J. Mater. Chem. A 4, 2856–2862. https://doi.org/10.1039/c5ta04136h

Chen, Y., Xiao, K., Shen, N., Zeng, R.J., Zhou, Y., 2018. Hydrogen production from a thermophilic alkaline waste activated sludge fermenter: Effects of solid retention time (SRT). Chemosphere 206, 101–106. https://doi.org/10.1016/j.chemosphere.2018.04.170

Chica, B., Wu, C.H., Liu, Y., Adams, M.W.W., Lian, T., Dyer, R.B., 2017. Balancing electron transfer rate and driving force for efficient photocatalytic hydrogen production in CdSe/CdS nanorod-[NiFe] hydrogenase assemblies. Energy Environ. Sci. 10, 2245–2255. https://doi.org/10.1039/c7ee01738c

Cho, H., Joo, H., Kim, H., Kim, J.E., Kang, K.S., Yoon, J., 2021. Improved photoelectrochemical properties of TiO_2 nanotubes doped with Er and effects on hydrogen production from water splitting. Chemosphere 267, 129289. https://doi.org/10.1016/j.chemosphere.2020.129289

Christoforidis, K.C., Fornasiero, P., 2017. Photocatalytic Hydrogen production: A rift into the future energy supply. ChemCatChem 9, 1523–1544. https://doi.org/10.1002/cctc.201601659

Chu, K.H., Ye, L., Wang, W., Wu, D., Chan, D.K.L., Zeng, C., Yip, H.Y., Yu, J.C.,

Wong, P.K., 2017. Enhanced photocatalytic hydrogen production from aqueous sulfide/sulfite solution by $ZnO_{0.6}S_{0.4}$ with simultaneous dye degradation under visible-light irradiation. Chemosphere 183, 219–228. https://doi.org/10.1016/j.chemosphere.2017.05.112

Corredor, J., Perez-Peña, E., Rivero, M.J., Ortiz, I., 2020a. Performance of rGO/TiO_2 photocatalytic membranes for hydrogen production. Membranes 10, 1–13. https://doi.org/10.3390/membranes10090218

Corredor, J., Rivero, M.J., Ortiz, I., 2020b. New insights in the performance and reuse of rGO/TiO_2 composites for the photocatalytic hydrogen production. Int. J. Hydrogen Energy (In press). https://doi.org/10.1016/j.ijhydene.2020.01.181

Corredor, J., Rivero, M.J., Rangel, C.M., Gloaguen, F., Ortiz, I., 2019. Comprehensive review and future perspectives on the photocatalytic hydrogen production. J. Chem. Technol. Biotechnol. 94, 3049–3063. https://doi.org/10.1002/jctb.6123

Ding, Y., Bertram, J.R., Eckert, C., Bommareddy, R.R., Patel, R., Conradie, A., Bryan, S., Nagpal, P., 2019. Nanorg Microbial Factories: Light-Driven Renewable Biochemical Synthesis Using Quantum Dot-Bacteria Nanobiohybrids. J. Am. Chem. Soc. 141, 10272–10282. https://doi.org/10.1021/jacs.9b02549

El-Khouly, M.E., El-Mohsnawy, E., Fukuzumi, S., 2017. Solar energy conversion: From natural to artificial photosynthesis. J. Photochem. Photobiol. C Photochem. Rev. 31, 36–83. https://doi.org/10.1016/j.jphotochemrev.2017.02.001

Elsayed, M.H., Jayakumar, J., Abdellah, M., Mansoure, T.H., Zheng, K., Elewa, A.M., Chang, C.-L., Ting, L.-Y., Lin, W.-C., Yu, H., Wang, W.-H., Chung, C.-C., Chou, H.-H., 2021. Visible-light-driven hydrogen evolution using nitrogen-doped carbon quantum dot-implanted polymer dots as metal-free photocatalysts. Appl. Catal. B

449 Environ. 283, 119659. https://doi.org/10.1016/j.apcatb.2020.119659

450 Fang, X., Cui, L., Pu, T., Song, J., Zhang, X., 2018. Core-shell CdS@MnS nanorods as
451 highly efficient photocatalysts for visible light driven hydrogen evolution. Appl.
452 Surf. Sci. 457, 863–869. https://doi.org/10.1016/j.apsusc.2018.07.012

453 Fukuzumi, S., Lee, Y.M., Nam, W., 2018. Thermal and photocatalytic production of
454 hydrogen with earth-abundant metal complexes. Coord. Chem. Rev. 355, 54–73.
455 https://doi.org/10.1016/j.ccr.2017.07.014

456 Gong, K., Zeng, Y., Kelley, D.F., 2013. Extinction coefficients, oscillator strengths, and
457 radiative lifetimes of CdSe, CdTe, and CdTe/CdSe nanocrystals. J. Phys. Chem. C
458 117, 20268–20279. https://doi.org/10.1021/jp4065449

459 Goy, R., Bertini, L., Rudolph, T., Lin, S., Schulz, M., Zampella, G., Dietzek, B.,
460 Schacher, F.H., De Gioia, L., Sakai, K., Weigand, W., 2017. Photocatalytic
461 Hydrogen Evolution Driven by [FeFe] Hydrogenase Models Tethered to Fluorene
462 and Silafluorene Sensitizers. Chem. Eur. J. 23, 334–345.
463 https://doi.org/10.1002/chem.201603140

464 Greene, B.L., Joseph, C.A., Maroney, M.J., Dyer, R.B., 2012. Direct evidence of active-
465 site reduction and photodriven catalysis in sensitized hydrogenase assemblies. J.
466 Am. Chem. Soc. 134, 11108–11111. https://doi.org/10.1021/ja3042367

467 Hamon, C., Ciaccafava, A., Infossi, P., Puppo, R., Even-Hernandez, P., Lojou, E.,
468 Marchi, V., 2014. Synthesis and enzymatic photo-activity of an O_2tolerant
469 hydrogenase-CdSe@CdS quantum rod bioconjugate. Chem. Commun. 50, 4989–
470 4992. https://doi.org/10.1039/c3cc49368g

471 Hemming, E.B., Chan, B., Turner, P., Corcilius, L., Price, J.R., Gardiner, M.G.,

Masters, A.F., Maschmeyer, T., 2018. [Fe(C_5Ar_5)$(CO)_2$Br] complexes as hydrogenase mimics for the catalytic hydrogen evolution reaction. Appl. Catal. B Environ. 223, 234–241. https://doi.org/10.1016/j.apcatb.2017.04.053

Hinojosa-Reyes, M., Camposeco-Solís, R., Zanella, R., Rodríguez González, V., 2017. Hydrogen production by tailoring the brookite and Cu_2O ratio of sol-gel Cu-TiO_2 photocatalysts. Chemosphere 184, 992–1002. https://doi.org/10.1016/j.chemosphere.2017.06.066

Holladay, J.D., Hu, J., King, D.L., Wang, Y., 2009. An overview of hydrogen production technologies. Catal. Today 139, 244–260. https://doi.org/10.1016/j.cattod.2008.08.039

Jasieniak, J., Califano, M., Watkins, S.E., 2011. Size-dependent valence and conduction band-edge energies of semiconductor nanocrystals. ACS Nano 5, 5888–5902. https://doi.org/10.1021/nn201681s

Jian, J.-X., Ye, C., Wang, X.-Z., Wen, M., Li, Z.-J., Li, X.-B., Chen, B., Tung, C.-H., Wu, L.-Z., 2016. Comparison of H_2 photogeneration by [FeFe]-hydrogenase mimics with CdSe QDs and Ru$(bpy)_3Cl_2$ in aqueous solution. Energy Environ. Sci. 9, 2083–2089. https://doi.org/10.1039/C6EE00629A

Jian, J.X., Liu, Q., Li, Z.J., Wang, F., Li, X.B., Li, C.B., Liu, B., Meng, Q.Y., Chen, B., Feng, K., Tung, C.H., Wu, L.Z., 2013. Chitosan confinement enhances hydrogen photogeneration from a mimic of the diiron subsite of [FeFe]-hydrogenase. Nat. Commun. 4, 2695. https://doi.org/10.1038/ncomms3695

Lai, G.J., Lyu, L.M., Huang, Y.S., Lee, G.C., Lu, M.P., Perng, T.P., Lu, M.Y., Chen, L.J., 2021. Few-layer WS_2–MoS_2 in-plane heterostructures for efficient photocatalytic hydrogen evolution. Nano Energy 81, 105608.

https://doi.org/10.1016/j.nanoen.2020.105608

Lewis S. Nathan, 2016. Research opportunities to advance solar energy utilization. Science 351, aad1920. https://doi.org/10.1126/science.aad1920.22

Li, C.B., Li, Z.J., Yu, S., Wang, G.X., Wang, F., Meng, Q.Y., Chen, B., Feng, K., Tung, C.H., Wu, L.Z., 2013. Interface-directed assembly of a simple precursor of [FeFe]-H2ase mimics on CdSe QDs for photosynthetic hydrogen evolution in water. Energy Environ. Sci. 6, 2597–2602. https://doi.org/10.1039/c3ee40992a

Li, R.X., Ren, X.T., Tang, M.Y., Chen, M.X., Huang, G.B., Fang, C.H., Liu, T., Feng, Z.H., Yin, Y.B., Guo, Y.M., Mei, S.K., Yan, J., 2018. Fabrication of covalently linked graphene-mediated [FeFe]-hydrogenases biomimetic photocatalytic hydrogen evolution system in aqueous solution. Appl. Catal. B Environ. 224, 772–782. https://doi.org/10.1016/j.apcatb.2017.09.062

Li, X., Wang, M., Chen, L., Wang, X., Dong, J., Sun, L., 2012. Photocatalytic water reduction and study of the formation of $Fe^{I}Fe^{0}$ species in diiron catalyst sytems. ChemSusChem 5, 913–919. https://doi.org/10.1002/cssc.201100490

Li, X.B., Jian, J.X., Wang, X.Z., Wang, Y., Xia, S.G., Tung, C.H., Wu, L.Z., 2020. Per-6-Thiol-Cyclodextrin Engineered [FeFe]-Hydrogenase Mimic/CdSe Quantum Dot Assembly for Photocatalytic Hydrogen Production. Sol. RRL (In press). https://doi.org/10.1002/solr.202000474

Liang, W.J., Wang, F., Wen, M., Jian, J.X., Wang, X.Z., Chen, B., Tung, C.H., Wu, L.Z., 2015. Branched polyethylenimine improves hydrogen photoproduction from a CdSe quantum dot/[FeFe]-hydrogenase mimic system in neutral aqueous solutions. Chem. Eur. J. 21, 3187–3192. https://doi.org/10.1002/chem.201406361

519 Liu, T., Darensbourg, M.Y., 2007. A mixed-valent, Fe(II)Fe(I), diiron complex
520 reproduces the unique rotated state of the [FeFe]hydrogenase active site. J. Am.
521 Chem. Soc. 129, 7008–7009. https://doi.org/10.1021/ja071851a

522 Lyon, E.J., Georgakaki, I.P., Reibenspies, J.H., Darensbourg, M.Y., 2001. Coordination
523 sphere flexibility of active-site models for Fe-only hydrogenase: Studies in intra-
524 and intermolecular diatomic ligand exchange. J. Am. Chem. Soc. 123, 3268–3278.
525 https://doi.org/10.1021/ja003147z

526 Mongin, C., Moroz, P., Zamkov, M., Castellano, F.N., 2018. Thermally activated
527 delayed photoluminescence from pyrenyl-functionalized CdSe quantum dots. Nat.
528 Chem. 10, 225–230. https://doi.org/10.1038/nchem.2906

529 Munfarida, S., Widayat, Satriadi, H., Cahyono, B., Hadiyanto, Philia, J., Prameswari, J.,
530 2020. Geothermal industry waste-derived catalyst for enhanced biohydrogen
531 production. Chemosphere 258, 127274.
532 https://doi.org/10.1016/j.chemosphere.2020.127274

533 Na, Y., Wang, M., Pan, J., Zhang, P., Åkermark, B., Sun, L., 2008. Visible light-driven
534 electron transfer and hydrogen generation catalyzed by bioinspired [2Fe2S]
535 complexes. Inorg. Chem. 47, 2805–2810. https://doi.org/10.1021/ic702010w

536 Nasir, M.S., Yang, G., Ayub, I., Wang, S., Wang, L., Wang, X., Yan, W., Peng, S.,
537 Ramakarishna, S., 2019. Recent development in graphitic carbon nitride based
538 photocatalysis for hydrogen generation. Appl. Catal. B Environ. 257, 117855.
539 https://doi.org/10.1016/j.apcatb.2019.117855

540 Nikolaidis, P., Poullikkas, A., 2017. A comparative overview of hydrogen production
541 processes. Renew. Sustain. Energy Rev. 67, 597–611.
542 https://doi.org/10.1016/j.rser.2016.09.044

Oh, W.C., Nguyen, D.C.T., Areerob, Y., 2020. Novel cadmium oxide-graphene nanocomposite grown on mesoporous silica for simultaneous photocatalytic H_2-evolution. Chemosphere 239, 124825. https://doi.org/10.1016/j.chemosphere.2019.124825

Orain, C., Quentel, F., Gloaguen, F., 2014. Photocatalytic Hydrogen Production Using Models of the Iron-Iron Hydrogenase Active Site Dispersed in Micellar Solution. ChemSusChem 7, 638–643. https://doi.org/10.1002/cssc.201300631

Pullen, S., Fei, H., Orthaber, A., Cohen, S.M., Ott, S., 2013. Enhanced photochemical hydrogen production by a molecular diiron catalyst incorporated into a metal-organic framework. J. Am. Chem. Soc. 135, 16997–17003. https://doi.org/10.1021/ja407176p

Putri, L.K., Ng, B.J., Ong, W.J., Lee, H.W., Chang, W.S., Mohamed, A.R., Chai, S.P., 2020. Energy level tuning of CdSe colloidal quantum dots in ternary 0D-2D-2D CdSe QD/B-rGO/O-gC_3N_4 as photocatalysts for enhanced hydrogen generation. Appl. Catal. B Environ. 265, 118592. https://doi.org/10.1016/j.apcatb.2020.118592

Quentel, F., Passard, G., Gloaguen, F., 2012. Electrochemical hydrogen production in aqueous micellar solution by a diiron benzenedithiolate complex relevant to [FeFe] hydrogenases. Energy Environ. Sci. 5, 7757–7761. https://doi.org/10.1039/c2ee21531d

Ribao, P., Alexandra Esteves, M., Fernandes, V.R., Rivero, M.J., Rangel, C.M., Ortiz, I., 2019. Challenges arising from the use of TiO_2/rGO/Pt photocatalysts to produce hydrogen from crude glycerol compared to synthetic glycerol. Int. J. Hydrogen Energy 44, 28494–28506. https://doi.org/https://doi.org/10.1016/j.ijhydene.2018.09.148

Rivero, M.J., Iglesias, O., Ribao, P., Ortiz, I., 2019. Kinetic performance of TiO_2/Pt/reduced graphene oxide composites in the photocatalytic hydrogen production. Int. J. Hydrogen Energy 44, 101–109. https://doi.org/10.1016/j.ijhydene.2018.02.115

Roy, S., Groy, T.L., Jones, A.K., 2013. Biomimetic model for [FeFe]-hydrogenase: asymmetrically disubstituted diiron complex with a redox-active 2,2′-bipyridyl ligand. Dalt. Trans. 42, 3843–3853. https://doi.org/10.1039/c2dt32457a

Sanchez, M.L.K., Sommer, C., Reijerse, E., Birrell, J.A., Lubitz, W., Dyer, R.B., 2019a. Investigating the Kinetic Competency of CrHydA1 [FeFe] Hydrogenase Intermediate States via Time-Resolved Infrared Spectroscopy. J. Am. Chem. Soc. 141, 16064–16070. https://doi.org/10.1021/jacs.9b08348

Sanchez, M.L.K., Wu, C.H., Adams, M.W.W., Dyer, R.B., 2019b. Optimizing electron transfer from CdSe QDs to hydrogenase for photocatalytic H_2 production. Chem. Commun. 55, 5579–5582. https://doi.org/10.1039/c9cc01150a

Seadira, T.W.P., Sadanandam, G., Ntho, T., Masuku, C.M., Scurrell, M.S., 2018. Preparation and characterization of metals supported on nanostructured TiO_2 hollow spheres for production of hydrogen via photocatalytic reforming of glycerol. Appl. Catal. B Environ. 222, 133–145. https://doi.org/10.1016/j.apcatb.2017.09.072

Shen, M., Jia, W., You, Y., Hu, Y., Li, F., Tian, S., Li, J., Jin, Y., Han, D., 2013. Luminescent properties of CdTe quantum dots synthesized using 3-mercaptopropionic acid reduction of tellurium dioxide directly. Nanoscale Res. Lett. 8, 1–6. https://doi.org/10.1186/1556-276x-8-253

Song, X.W., Wen, H.M., Ma, C.B., Hu, M.Q., Chen, H., Cui, H.H., Chen, C.N., 2014.

591 Photocatalytic hydrogen evolution by two comparable [FeFe]-hydrogenase mimics
592 assembled to the surface of ZnS. Appl. Organomet. Chem. 28, 267–273.
593 https://doi.org/10.1002/aoc.3119

594 Stern, O., Volmer, M., 1919. Über die Abklingzeit der Fluoreszenz. Z. Phys. 20, 183–
595 188.

596 Streich, D., Astuti, Y., Orlandi, M., Schwartz, L., Lomoth, R., Hammarström, L., Ott,
597 S., 2010. High-turnover photochemical hydrogen production catalyzed by a model
598 complex of the [FeFe]-hydrogenase active site. Chem. Eur. J. 16, 60–63.
599 https://doi.org/10.1002/chem.200902489

600 Stripp, S.T., Happe, T., 2009. How algae produce hydrogen—news from the
601 photosynthetic hydrogenase. Dalt. Trans. 9960–9969.
602 https://doi.org/10.1039/b916246a

603 Supplis, C., Gros, F., Dahi, G., Dauchet, J., Roudet, M., Gloaguen, F., Cornet, J.F.,
604 2018. Spectral radiative analysis of bio-inspired H_2 production in a benchmark
605 photoreactor: A first investigation using spatial photonic balance. Int. J. Hydrogen
606 Energy 43, 8221–8231. https://doi.org/10.1016/j.ijhydene.2018.03.097

607 Trincado, M., Banerjee, D., Grützmacher, H., 2014. Molecular catalysts for hydrogen
608 production from alcohols. Energy Environ. Sci. 7, 2464-2503.
609 https://doi.org/10.1039/c4ee00389f

610 Troppmann, S., König, B., 2016. Functionalized Vesicles with Co-Embedded CdSe
611 Quantum Dots and [FeFe]-Hydrogenase Mimic for Light-Driven Hydrogen
612 Production. ChemistrySelect 1, 1405–1409. https://doi.org/10.1002/slct.201600032

613 Tu, Y.J., Njus, D., Schlegel, H.B., 2017. A theoretical study of ascorbic acid oxidation

and HOO•/$O_2^{•-}$ Radical scavenging. Org. Biomol. Chem. 15, 4417–4431. https://doi.org/10.1039/c7ob00791d

Wang, F., Liang, W.J., Jian, J.X., Li, C.B., Chen, B., Tung, C.H., Wu, L.Z., 2013. Exceptional poly(acrylic acid)-based artificial [FeFe]-hydrogenases for photocatalytic H_2 production in water. Angew. Chemie Int. Ed. 52, 8134–8138. https://doi.org/10.1002/anie.201303110

Wang, F., Wang, W.G., Wang, H.Y., Si, G., Tung, C.H., Wu, L.Z., 2012. Artificial photosynthetic systems based on [FeFe]-hydrogenase mimics: The road to high efficiency for light-driven hydrogen evolution. ACS Catal. 2, 407–416. https://doi.org/10.1021/cs200458b

Wang, F., Wang, W.G., Wang, X.J., Wang, H.Y., Tung, C.H., Wu, L.Z., 2011. A highly efficient photocatalytic system for hydrogen production by a robust hydrogenase mimic in an aqueous solution. Angew. Chemie Int. Ed. 50, 3193–3197. https://doi.org/10.1002/anie.201006352

Wang, H.-Y., Wang, W.-G., Si, G., Wang, F., Tung, C.-H., Wu, L.-Z., 2010. Photocatalytic Hydrogen Evolution from Rhenium(I) Complexes to [FeFe] Hydrogenase Mimics in Aqueous SDS Micellar Systems: A Biomimetic Pathway. Langmuir 26, 9766–9771. https://doi.org/10.1021/la101322s

Wang, M., Han, K., Zhang, S., Sun, L., 2015. Integration of organometallic complexes with semiconductors and other nanomaterials for photocatalytic H_2 production. Coord. Chem. Rev. https://doi.org/10.1016/j.ccr.2014.12.005

Wang, P., Zhang, J., He, H., Xu, X., Jin, Y., 2015. The important role of surface ligand on CdSe/CdS core/shell nanocrystals in affecting the efficiency of H_2 photogeneration from water. Nanoscale 7, 5767–5775.

https://doi.org/10.1039/c4nr07343f

Wang, W., Song, X.W., Hong, Z., Li, B., Si, Y., Ji, C., Su, K., Tan, Y., Ju, Z., Huang, Y., Chen, C.N., Yuan, D., 2019. Incorporation of iron hydrogenase active sites into a stable photosensitizing metal-organic framework for enhanced hydrogen production. Appl. Catal. B Environ. 258, 117979. https://doi.org/10.1016/j.apcatb.2019.117979

Wen, M., Li, X.B., Jian, J.X., Wang, X.Z., Wu, H.L., Chen, B., Tung, C.H., Wu, L.Z., 2016. Secondary coordination sphere accelerates hole transfer for enhanced hydrogen photogeneration from [FeFe]-hydrogenase mimic and CdSe QDs in water. Sci. Rep. 6, 29851. https://doi.org/10.1038/srep29851

Wen, M., Wu, H.-L., Jian, J.-X., Wang, X.-Z., Li, X.-B., Chen, B., Tung, C.-H., Wu, L.-Z., 2017. Integrating CdSe Quantum Dots with a [FeFe]-Hydrogenase Mimic into a Photocathode for Hydrogen Evolution at a Low Bias Voltage. ChemPhotoChem 1, 260–264. https://doi.org/10.1002/cptc.201700041

Wittkamp, F., Senger, M., Stripp, S.T., Apfel, U.P., 2018. [FeFe]-Hydrogenases: Recent developments and future perspectives. Chem. Commun. 54, 5934–5942. https://doi.org/10.1039/c8cc01275j

Wroblewska-Wolna, A.M., Harvie, A.J., Rowe, S.F., Critchley, K., Butt, J.N., Jeuken, L.J.C., 2020. Quantum dot interactions with and toxicity to Shewanella oneidensis MR-1. Nanotechnology 31, 134005. https://doi.org/10.1088/1361-6528/ab5f78

Yang, J., Miao, H., Jing, J., Zhu, Y., Choi, W., 2021. Photocatalytic activity enhancement of PDI supermolecular via π-π action and energy level adjusting with graphene quantum dots. Appl. Catal. B Environ. 281, 119547. https://doi.org/10.1016/j.apcatb.2020.119547

662 Yang, Y., Zhou, C., Wang, W., Xiong, W., Zeng, G., Huang, D., Zhang, C., Song, B.,
663 Xue, W., Li, X., Wang, Z., He, D., Luo, H., Ouyang, Z., 2021. Recent advances in
664 application of transition metal phosphides for photocatalytic hydrogen production.
665 Chem. Eng. J. 405, 126547. https://doi.org/10.1016/j.cej.2020.126547

666 Yu, T., Zeng, Y., Chen, J., Li, Y.Y., Yang, G., Li, Y., 2013. Exceptional dendrimer-
667 based mimics of diiron hydrogenase for the photochemical production of
668 hydrogen. Angew. Chemie Int. Ed. 52, 5631–5635.
669 https://doi.org/10.1002/anie.201301289

670 Yu, W.W., Qu, L., Guo, W., Peng, X., 2003. Experimental determination of the
671 extinction coefficient of CdTe, CdSe, and CdS nanocrystals. Chem. Mater. 15,
672 2854–2860. https://doi.org/10.1021/cm034081k

673 Yue, D., Qian, X., Kan, M., Ren, M., Zhu, Y., Jiang, L., Zhao, Y., 2017. Sulfurated
674 [NiFe]-based layered double hydroxides nanoparticles as efficient co-catalysts for
675 photocatalytic hydrogen evolution using CdTe/CdS quantum dots. Appl. Catal. B
676 Environ. 209, 155–160. https://doi.org/10.1016/j.apcatb.2017.02.075

677 Zamkov, M., 2017. Solar hydrogen generation: Exceeding 100% efficiency. Nat.
678 Energy 2, 17072. https://doi.org/10.1038/nenergy.2017.72

679